ARTICLE

A hydro-environmental watershed model improved in canal-aquifer water exchange process

Chie Imagawa · Junichiro Takeuchi ·
Toshihiko Kawachi · Kei Ishida ·
Shunsuke Chono · Natsuki Buma

Abstract Long-term simulation using the distributed hydro-environmental watershed model is efficacious for assessing irrigation impacts on hydrological cycle in detail and for implementing watershed management successfully. In this article, the previously developed hydro-environmental watershed model (HEWM-1) is improved in the water exchange process caused by surface water-groundwater interaction via drainage canals and/or underdrains. The time-varying stream flow in canals is described by the complete one-dimensional shallow water equations in a newly introduced submodel, the open channel flow submodel. This submodel coordinates with the other submodels: the tank, soil moisture and groundwater flow submodels which are interlinked in a cascade manner. The improved model (HEWM-2) is applied to an agricultural watershed covering an area from an alluvial fan onto a nearly level alluvial plain, to be validated. The simulation by HEWM-2 is informative for identifying whether any drainage canal is gaining or losing water in relation to groundwater level. It could thus provide useful information for conserving a complex network of drainage canals which also functions as a passage for aquatic animals like fishes.

C. Imagawa (✉) · J. Takeuchi · T. Kawachi · K. Ishida ·
S. Chono · N. Buma
Graduate School of Agriculture, Kyoto University,
Kitashirakawa Oiwake-cho, Sakyo-ku, Kyoto 606-8502, Japan
e-mail: chieima@kais.kyoto-u.ac.jp

Introduction

In a regional hydrological cycle, surface water and groundwater interact to exchange water across their common boundary. In an alluvial fan where groundwater level is adequately below the ground surface, the dominant effect of water exchange is the groundwater recharge from the surface. On the other hand, in an alluvial plain where groundwater level is relatively close to the ground surface, both groundwater recharge and groundwater discharge could occur via rivers and canals. While running from an alluvial fan to the following alluvial plain, a stream generally loses water to aquifer in certain upper reaches and gains water from aquifer in lower reaches. Even in the same reach, a stream could also switch between gaining and losing across the seasons according to the rise and fall of the difference between surface water level and groundwater level. The dynamic processes of groundwater system and stream–aquifer interaction are affected not only by geological/meteorological conditions but also by human activities such as irrigation. Studies and clear understanding of the dynamic stream–aquifer interaction would provide some guidelines for reasonable water management and ecological prevention.

One of the approaches to quantify a stream–aquifer flow is to utilize a hydrological watershed model (e.g. Hu et al. 2007; Krause and Bronstert 2007). In many hydrological watershed models, a stream–aquifer flow is usually considered as a water flux through a low-permeable streambed stratum (e.g. Rushton and Tomlinson 1979). The MOD-FLOW (McDonald and Harbaugh 1988) and the stream-flow routing packages such as RIV (McDonald and Harbaugh 1988), STR1 (Prudic 1989) and SFR1 (Prudic 2004) have been coupled with some surface runoff models to quantify a stream–aquifer flow. Kim et al. (2008)

developed SWAT-MODFLOW model and applied it to estimate groundwater drawdown and stream flow reduction by pumping groundwater out. Other hydrological watershed models (e.g. Jia et al. 2001; Korkmaz et al. 2009) have adopted the expression similar to the streamflow routing packages. Jia et al. (2001) developed the WEP model, which simulates water and energy cycles in a watershed, and applied it to project water balance change by urbanization in the future. Korkmaz et al. (2009) adopted MODCOU to reproduce the damaging flood that was caused by immense groundwater discharge. These studies suggest that the expression similar to the streamflow routing packages is useful and relevant for quantifying a stream–aquifer flow. These studies, however, make rough estimates of unsteady surface water levels in streams. The stream flow is approximated with kinematic wave flow (Jia et al. 2001) or steady uniform flow (Kim et al. 2008; Korkmaz et al. 2009).

For reliable estimation of a stream–aquifer flow, spatiotemporal variation of the surface water level should be considered, especially for a stream running in an alluvial plain. For description of the surface water flow dynamics, the complete (non-approximated) shallow water equations (i.e. unsteady open channel flow equations) are proper. Swain and Wexler (1996) developed a coupled surface water and groundwater flow model (MODBRANCH) for simulation of stream–aquifer flow. Their model links MODFLOW to BRANCH (Schaffranek et al. 1981) in which the shallow water equations are used to simulate unsteady flow dynamics in an open channel network. Thompson et al. (2004) adopted MIKE-11, which is based on the shallow water equations and is able to simulate the flow through hydraulic structures such as weirs, gates, bridges and culverts, to link it with MIKE-SHE. Their linked model was applied to low-lying wet grassland to investigate the seasonal variations of groundwater level and surface water level in a ditch. These attempts indeed vouch for the necessity of employing unsteady surface water flow model for representing stream flow which interact with aquifers, but do not deal with stream–aquifer interaction induced by irrigation and drainage practices.

In an agricultural watershed, surface water and groundwater interaction is often promoted by human-induced surface/subsurface water modifications such as irrigation and drainage. Many previous studies (e.g. Fujihara and Ohashi 2000; Liu et al. 2005; Imaizumi et al. 2006) indicated that infiltration from the irrigated paddy fields makes a large contribution to groundwater recharge. Infiltration from irrigation and drainage canals is also a non-negligible source of groundwater recharge (Fujinawa 1981; Wakasa 2006). In agricultural lowland area, drainage canals play an important role in groundwater discharge from shallow aquifers to keep soil water contents proper in crop fields.

Carroll et al. (2010) developed a MODFLOW-based hydrological model in which the water exchange between drainage canals and aquifer is focused on but the canal flow is assumed to be steady and uniform. Takeuchi et al. (2009) developed a finite-volume hydro-environmental model in which the water exchange between drainage canals and aquifer is taken into account. Takeuchi et al. (2010) constructed the refined hydro-environmental watershed model (HEWM-1) that enables more reliable estimation of canal-aquifer flow with the high-resolution divisions of the watershed. Both of them make a rigid-lid assumption for water level in any canal, thus prescribing time-independent in-canal water levels as internal boundary conditions.

This study aims at developing a hydro-environmental watershed model that can simulate the dynamic canal-aquifer flow caused by the rise and fall of the difference between surface water level and groundwater level. For attaining this purpose, this study makes HEWM-1 (Takeuchi et al. 2010) free from the assumption that in-canal water levels are time-independent. The time-varying stream flow in canals is described by the complete one-dimensional (1-D) shallow water equations without any approximations. Different two effects of canal-aquifer flow are separately considered: exchange flow through canal bed that is according to the difference in hydraulic head between canal and aquifer and groundwater discharge through underdrains that is caused by removing superfluous soil water in farmlands. The presently improved model (HEWM-2) is applied to a mesoscale agricultural watershed including lowland areas to be validated. With a long-term simulation by HEWM-2, the spatiotemporal variations of canal-aquifer flow and their contribution to the overall water budget are estimated.
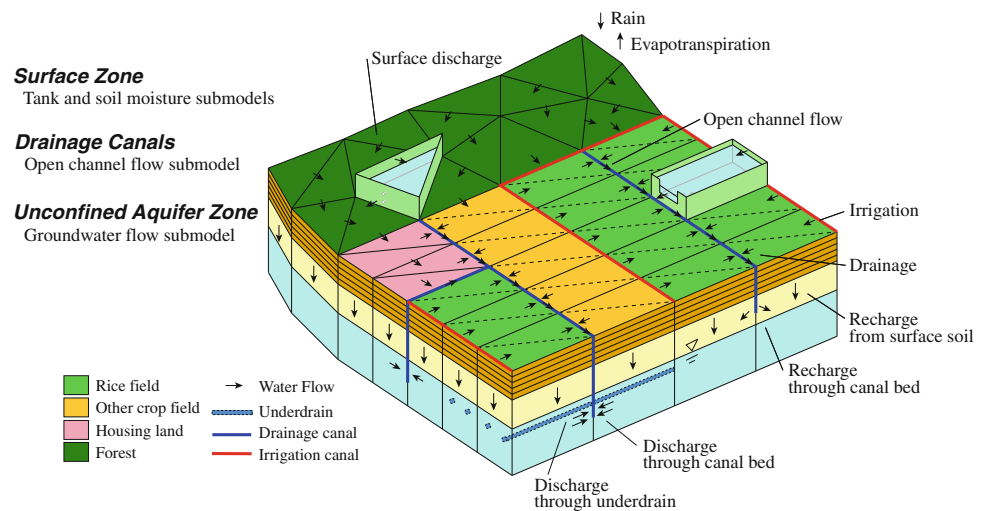
Model development

Model structure

The graphical representation of the improved hydro-environmental model, HEWM-2, is shown in Fig. 1. In HEWM-2, as in HWEM-1, watershed geometry is subdivided into column cells which have triangular tops that well fit field plots and canal courses. Profile of a column cell is zoned into two: a surface zone and an unconfined aquifer zone. Hydrological process in the surface zone is expressed by combining a tank submodel and a soil moisture submodel according to Alam et al. (2006), and that in the unconfined aquifer zone is expressed by a shallow groundwater flow submodel.

A major improvement over HWEM-1 is made for treating flow in agricultural drainage canals as unsteady open channel flow, in lieu of steady flow with rigid-lid

Fig. 1 Schematic of hydro-environmental watershed model (HEWM-2)

Surface Zone
Tank and soil moisture submodels

Drainage Canals
Open channel flow submodel

Unconfined Aquifer Zone
Groundwater flow submodel

Rice field — Water Flow
Other crop field ⋯ Underdrain
Housing land — Drainage canal
Forest — Irrigation canal

assumption. Another improvement is made for realistic and detailed representation of the water exchange between drainage canals and aquifer. In HEWM-2, the canal-aquifer flow rate is defined as the sum of the exchange flow rate through canal bed and the underdrain discharge.

Surface zone

The tank submodel expresses the hydrological processes on the ground surface, relating surface water storage of effective rainfall, infiltration, evaporation, inflow from upper tanks and outflow to a lower tank. In farmland areas, one tank is assigned to one set of cells identical with one field plot, whereas in other off-field areas, one tank is assigned to one cell. On a paddy field tank, the outflow from the tank is represented by an overflow through a sharp-crested weir whose height is identified to actual weir height of an outlet at a field plot. On a non-paddy field tank, the outflow from the tank is calculated in the same way as that from the standard tank model (Sugawara et al. 1986). The infiltration through the ground surface is calculated with the soil moisture submodel as described in the following paragraph. The evaporation occurs from the surface tank when the surface water storage is not null. The potential evaporation is the product of a drop coefficient and the pan evaporation, which is estimated by use of the Penman method.

A soil moisture model, which was originally developed for a lumped runoff model (Tan and O'Connor 1996), is adapted for a submodel in this distributed watershed model. The soil moisture submodel expresses the hydrological processes in the unsaturated subsurface soil, relating soil water retention, infiltration, evapotranspiration, lateral outflow and vertical percolation. The infiltration is regulated by soil water content so that the limited water

infiltrates under a wet condition. The surplus water to the infiltration remains in the surface tank. The soil water content is retained to a certain capacity, and the surplus water to the capacity is separated into a lateral outflow and a vertical percolation. The evapotranspiration occurs in the subsurface soil only when the surface water storage is less than the potential evaporation. Also the evapotranspiration rate is regulated by soil water content so that the limited soil water is pulled off under a dry condition.

The lateral outflows from the ground surface and the subsurface soil are discharged into drainage canals. If a cell abuts on no canal, the outflow from the cell is given as an inflow contribution to the lowest cell amongst the neighbouring three cells. The vertical percolation from subsurface soil recharges the groundwater in the aquifer zone.

A minor improvement on HWEM-1 is made in making a distinction between snowfall and rainfall. From air temperature and relative humidity, whether precipitation is rainfall, snowfall, or sleety rainfall is inferred. The following two threshold values for relative humidity are criteria of distinction (Matsuo 1984).

$$H_s = -7.5T + 93 \quad (0.0 \leq T < 5.0) \tag{1}$$

$$H_r = 46\sqrt{6.2 - T} \quad (1.47 \leq T < 4.57) \tag{2}$$

where T is the air temperature (°C), H_s is the threshold relative humidity (%) for distinction between snow and sleet and H_r is that (%) for distinction between rain and sleet. The type of precipitation is identified to be snowfall if the air temperature is under 0°C or the relative humidity is less than H_s even if the air temperature is over 0°C, or to be rainfall if the air temperature is over 5°C or the relative humidity is more than H_r even if the air temperature is under 5°C. If the relative humidity is between the two threshold values, the precipitation is regarded as a half-and-half sleety mixture of snow and rain.

The melting rate of snow is essentially determined by a heat balance on a surface of snow cover. However, an empirical expression that relates the melting rate to only air temperature is usually used for estimating the amount of melting. Here, the following degree-hour method (Kojima et al. 1983) is employed.

$$M = m \sum_{i=1}^{24} \max\left(0.0, T_i^h\right) \qquad (3)$$

where M is the rate of snow melting (mm/day), T^h is the hourly-mean air temperature (°C) and m is the melting coefficient (mm/(°C day)).

Drainage canals

The unsteady open channel flow submodel for drainage canals is described by the following set of the continuity and momentum equations, which is defined in 1-D domain Ω_r.

$$\frac{\partial A}{\partial t} + \frac{\partial Q}{\partial \zeta} = q_{in} \qquad (4)$$

$$\frac{\partial Q}{\partial t} + \frac{\partial}{\partial \zeta}\left(\frac{\beta Q^2}{A}\right) = -gA\frac{\partial}{\partial \zeta}(h_r + z_r) - gAS_f \qquad (5)$$

with

$$S_f = \frac{n_M^2 Q|Q|}{A^2 R^{4/3}} \qquad (6)$$

where A is the wetted cross-sectional area (m²), Q is the volumetric flow rate (m³/s), ζ is the local curvilinear abscissa along the channel bed, q_{in} is the lateral inflow per unit width (m²/s), β is the Boussinesq coefficient, h_r is the water depth (m), z_r is the elevation of the channel bed, g is the gravitational acceleration (m/s²), S_f is the friction slope that is estimated with the Manning's equation, n_M is the Manning's roughness coefficient and R is the hydraulic radius (m). The lateral inflow in the continuity equation is assumed to bring no momentum because its direction is considered to be at right angle to the channel flow. The sources of the lateral inflow are tributaries, intakes for irrigation water supply, surface discharge and canal-aquifer flow rate. The surface discharge is that calculated from the surface tank and soil moisture submodels. The canal-aquifer flow rate is calculated in linking the unsteady open channel flow submodel with the shallow groundwater flow submodel.

The initial condition is given as follows.

$$h_r(\zeta, 0) = h_{r0}(\zeta) \quad \text{in} \quad \Omega_r \qquad (7)$$

where h_{r0} is the prescribed initial water depth (m) over the whole domain Ω_r. At the upstream end of the canal, the prescribed volumetric flow rate, Q^{up} (m³/s), is given.

$$Q(\zeta, t) = Q^{up}(t) \quad \text{on} \ \Gamma^{up} \qquad (8)$$

where Γ^{up} is the upstream boundary. At the downstream end of the canal, the prescribed water depth, h_r^{dw} (m), is given if flow in the canal is under the backwater influence of river or lake which communicates with it.

$$h_r(\zeta, t) = h_r^{dw}(t) \quad \text{on} \ \Gamma_L^{dw} \qquad (9)$$

where Γ_L^{dw} is the backwater-type downstream boundary. If the canal end is a drop, the critical water depth, h_c^{dw} (m) and the null flow rate flux are given for subcritical and supercritical flows in the canal, respectively.

$$\begin{cases} h_r(\zeta, t) = h_c^{dw}(t) & \text{if } h_r \geq h_c^{dw} \\ \frac{\partial Q}{\partial \zeta} = 0 & \text{if } h_r < h_c^{dw} \end{cases} \text{on} \quad \Gamma_F^{dw} \qquad (10)$$

where Γ_F^{dw} is the drop-type downstream boundary.

Gate or weir across the canal is treated as an internal boundary where the flow rate, Q_g, expressed by well-defined flow rate formula, is prescribed.

$$Q(\zeta, t) = Q_g(t) \quad \text{on} \ \Gamma^{in} \qquad (11)$$

where Γ^{in} is the internal boundary.

The 1-D shallow water equations (Eqs. 4, 5) are numerically solved with the finite difference method in space and the Runge-Kutta method in time. The spatial discretization of the canals is adjusted to that of the surface zone so that length of a subdivided canal is identical to that of a side of a triangular cell. The convection term in the momentum equation that, if it is dominant, may render the solution oscillatory is numerically approximated resorting to the upwind scheme, adding an artificial viscosity into the equation (Asai and Hosoda 1999).

Aquifer zone

The shallow groundwater flow submodel expresses the unsteady groundwater flow in the unconfined aquifer zone that lies on a low-permeable layer. The shallow groundwater flow dynamics is predominantly two-dimensional and expressed by the following equation with the Dupuit's assumption.

$$n_e \frac{\partial H_g}{\partial t} = -\nabla \cdot \left(-(H_g - z_b)K\nabla H_g\right) + r_g(\mathbf{x}, t - t_d) - l \\ - q_{dc} - q_{ud} \qquad (12)$$

where n_e is the effective porosity, H_g is the groundwater level (m), z_b is the elevation (m) of the low-permeable layer, K is the saturated hydraulic conductivity (m/s), r_g is the recharge (m/s) from the surface zone, t_d is the time lag, l is the leakage (m/s) to a deeper layer which is assumed to be proportional to the water depth in the
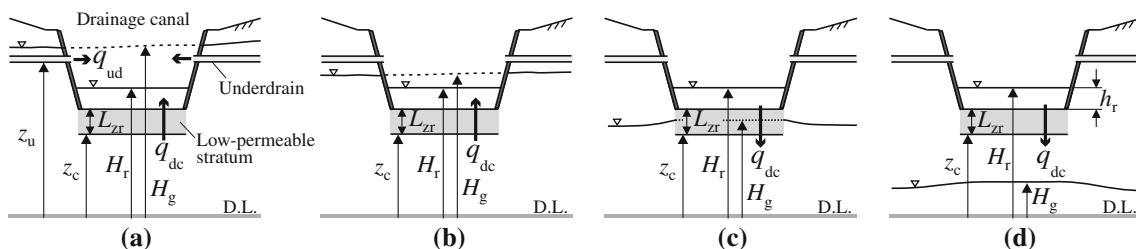
Fig. 2 Interactive canal-aquifer flow. (**a–c** connected conditions, **d** disconnected condition)

aquifer zone, q_{dc} is the exchange flow rate (m/s) through canal bed per unit wetted-area (positive and negative values indicate the flow into and out of the canal, respectively), q_{ud} is the underdrain discharge (m/s) per unit surface-cell area and $\mathbf{x} = (x, y)^T$ is the Cartesian coordinate system.

The exchange flow rate through canal bed is expressed as a water flux through a low-permeable streambed stratum. The water flux is calculated on the basis of the Darcy's law, represented by a product of hydraulic conductivity of the low-permeable streambed stratum and hydraulic gradient between top and bottom of the stratum (Prickett and Lonnquist 1971).

If $h_r > 0$,

$$q_{dc} = \begin{cases} K_{zr}\dfrac{(H_g - H_r)}{L_{zr}}, & \text{if } z_c \leq H_g \\ K_{zr}\dfrac{(z_c - H_r)}{L_{zr}}, & \text{if } H_g < z_c \end{cases} \quad (13)$$

If $h_r = 0$,

$$q_{dc} = \begin{cases} K_{zr}\dfrac{(H_g - z_r)}{L_{zr}}, & \text{if } z_r \leq H_g \\ 0, & \text{if } H_{g < z_r} \end{cases} \quad (14)$$

where H_r ($= h_r + z_r$) is the surface water level (m) in the canal, L_{zr} is the thickness (m) of the low-permeable canal bed stratum that is hypothetically placed, K_{zr} is the hydraulic conductivity (m/s) of the low-permeable canal bed stratum and z_c is the bottom elevation (m) of the canal bed stratum. Values of L_{zr} and K_{zr} are those to be identified through calibration of the model (Prudic 2004). It is assumed that canals with concrete-lined bed have no exchange flow through their beds. As Eq. 13 states, the exchange flow rate, q_{dc}, becomes independent of the time-dependent groundwater level when $H_g < z_c$ (or the groundwater table drops below the streambed-stratum bottom), but still varies in time since H_r is that obtained from unsteady streamflow routing.

The underdrain discharge can be expressed as

$$q_{ud} = \begin{cases} \kappa K(H_g - H_r), & \text{if } z_u \leq H_r, H_g \\ \kappa K(H_g - z_u), & \text{if } H_r < z_u \leq H_g \\ 0, & \text{if } H_g < z_u \leq H_r \\ 0, & \text{if } H_r, H_g < z_u \end{cases} \quad (15)$$

where z_u is the elevation (m) of the underdrain and κ is the discharge coefficient (m^{-1}) denoting drainage performance of the underdrain. Eq. 15 is only applied to farmlands provided with underdrains for soil moisture control.

As an example, all possible situations caused under a typical condition of for $h_r > 0$ and $H_r < z_u$ are illustrated in Fig. 2. The first three and the last denote the situations in that surface water and groundwater are connected and disconnected, respectively. As Eq. 13 states, surface water and groundwater are hydraulically connected and thus q_{dc} is a function of the difference between the surface water level and the groundwater level, when $H_g > z_c$. When $H_g < z_c$, groundwater is regarded as being hydraulically disconnected with surface water (Sophocleous 2002) and thus q_{dc} becomes independent of the time-dependent groundwater level. The relation of the canal-aquifer flow rate and the groundwater level for all the four conditions is shown in Fig. 3. In Cases (a) to (c), the canal-aquifer flow rate is proportional to the groundwater level. In Case
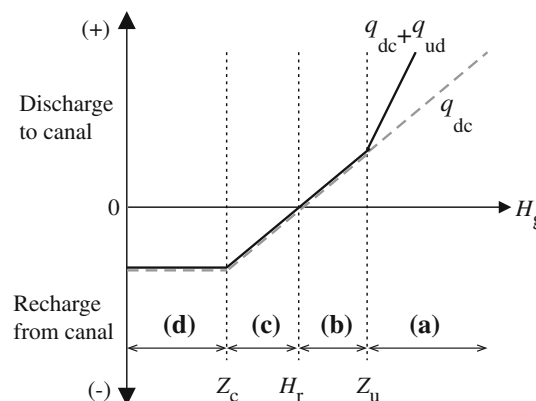
Fig. 3 Canal-aquifer flow rate as a function of groundwater level

(d), the canal-aquifer flow rate is independent of the groundwater level.

The following initial and boundary conditions are given for the unambiguous solution to the above equation.

$$H_g(\mathbf{x}, 0) = H_{g0}(\mathbf{x}) \quad \text{in } \Omega_g \tag{16}$$

$$H_g(\mathbf{x}, t) = H_g^D(\mathbf{x}, t) \quad \text{on } \Gamma_{wg}^D \tag{17}$$

$$-\left(H_g - z_b\right) K \frac{\partial H_g}{\partial v_{wg}} = q_{wg}(\mathbf{x}, t) \quad \text{on } \Gamma_{wg}^N \tag{18}$$

where H_{g0} is the prescribed initial groundwater level (m) over the whole domain Ω_g, H_g^D is the prescribed groundwater level (m) on the Dirichlet boundary Γ_{wg}^D, q_{wg} is the prescribed water flux per unit width (m²/s) through the Neumann boundary Γ_{wg}^N and v_{wg} is the unit vector outward normal to Γ_{wg}^N.

The shallow groundwater flow equation is numerically solved with the cell-based finite-volume method in space and the backward Euler method in time. When a computed groundwater level becomes higher than the ground level, the groundwater level is equalized to the ground level, and the surplus water is regarded as spring. The spring water is discharged to the drainage canals or the external boundaries. If a cell abuts on no canal, the spring water is given as an inflow contribution to the lowest cell amongst the neighbouring three cells.

Application

Study area

The study area is a part of Takashima City in Shiga Prefecture, Japan, being located on the northwestern side of Lake Biwa, as illustrated in Fig. 4. The area is in the Japan Sea climatic zone and has the average annual precipitation of 1,812 mm, 17% of which is snowfall (Japan Meteorological Agency 2011). The annual evapotranspiration is estimated at about 690 mm/y (Lake Biwa Research Institute 1988).

The study area of 12.7 km² wide is bordered with the Sakai River and the Ishida River on the northern and southern sides, respectively. The western boundary is the ridge separating watersheds, and the eastern is the shore of Lake Biwa. In the area, a variety of landforms can be found including forested hills (300–400 m AMSL), an alluvial fan formed by the Sakai River, river terraces along the Ishida River, valley floors and a nearly level alluvial plain (90 m AMSL). Figure 5 shows the hydrogeological profile, obtained from the core borings and the groundwater level observation, along the *Line A* depicted in Fig. 4. The inclination of the ground surface in the alluvial fan is about 0.04 and that in the alluvial plain is smaller than 0.01. Depth of the groundwater table below the ground surface is
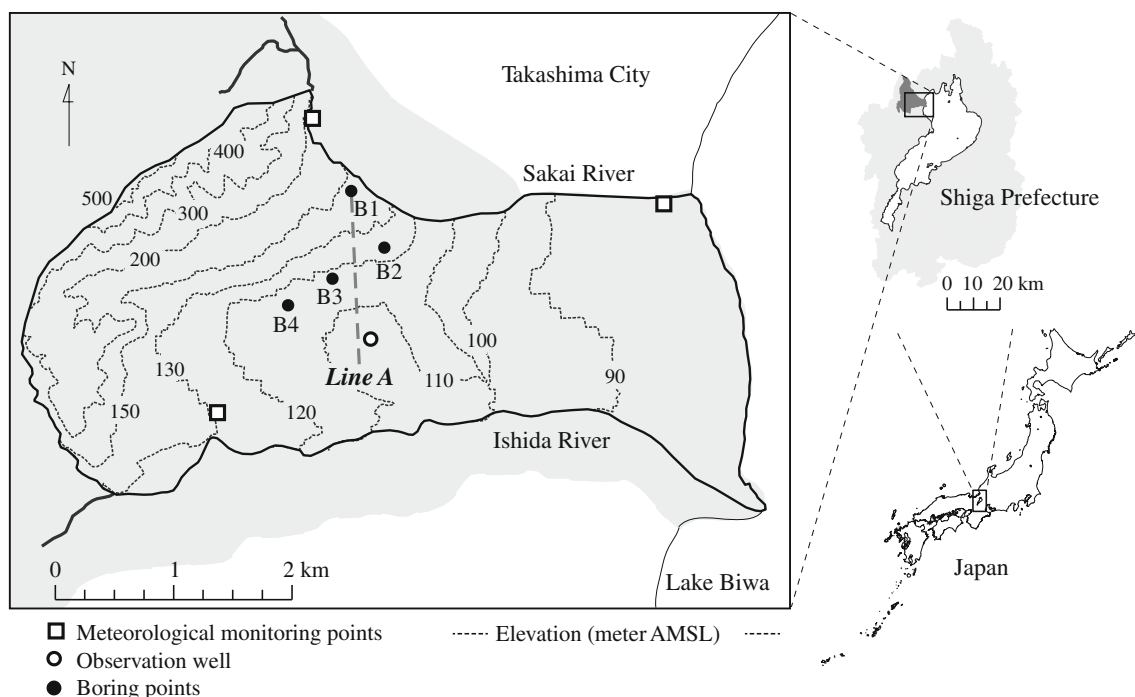
Fig. 4 Study area
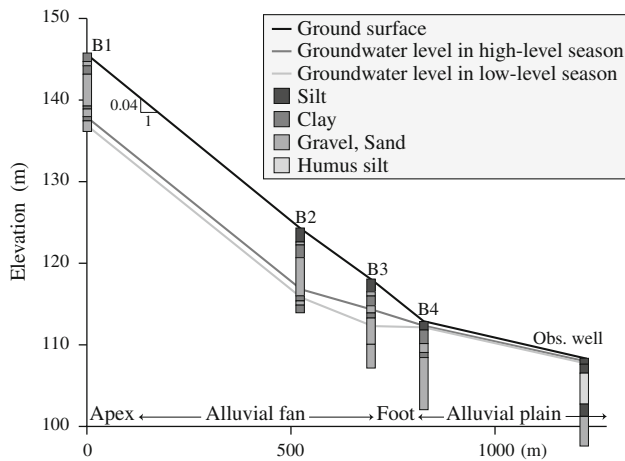
Fig. 5 Hydrogeological profile along *Line A*

8–15 m in the alluvial fan, while only 2 m or less in the alluvial plain. The groundwater table in the fan is, for the most part, along the ground surface, and getting close to the ground surface towards the foot of the fan. The geological columns of the boring cores for the alluvial fan mainly consist of sandy gravel, silt and clay, while for the alluvial plain mainly consist of humus silt and silt. The in situ permeability tests indicated that the sandy gravel in the alluvial fan has high hydraulic conductivity of 10^{-3} cm/s and the humus silt in the alluvial plain has low hydraulic conductivity of 10^{-4} cm/s.

The farmlands in the fan area were not suitable for rice cropping because subsurface water quickly percolates and

runs through the aquifer without supplying sufficient water to crops. The farmlands on the alluvial plain had been in ill-drained condition because of high groundwater level and backwater in canal from Lake Biwa. From 1970s to 1990s, the small field plots were altered to the large rectangular plots, the drainage canals were separated from the irrigation canals to improve drainage performance, and the underdrains were put to get rid of excess water in soil and keep low level of groundwater. In addition, the dredging of the main drainage canal which runs in the middle of the study area improved the drainage performance all over the area, and provided sufficient flow capacity against 10-year flood.

Forests, rice fields and other crop fields account for 33%, 33% and 10% of the entire area, respectively. The rice fields in the western part of the area are irrigated with water withdrawn from a branch of the Ishida River, some irrigation tanks, spring and a deep aquifer. The drainage water from those fields is collected into the main drainage canal. The water flowing down in the main drainage canal is reused as irrigation water for the rice fields in the eastern part of the area, which is also irrigated with return water pumped up from Lake Biwa.

Materials

The values of rainfall and pan evaporation on each cell were interpolated from those available at the monitoring points by the method of inverse squared distance weighting (Brath et al. 2004). The air temperature on each cell was

Fig. 6 Geological zoning
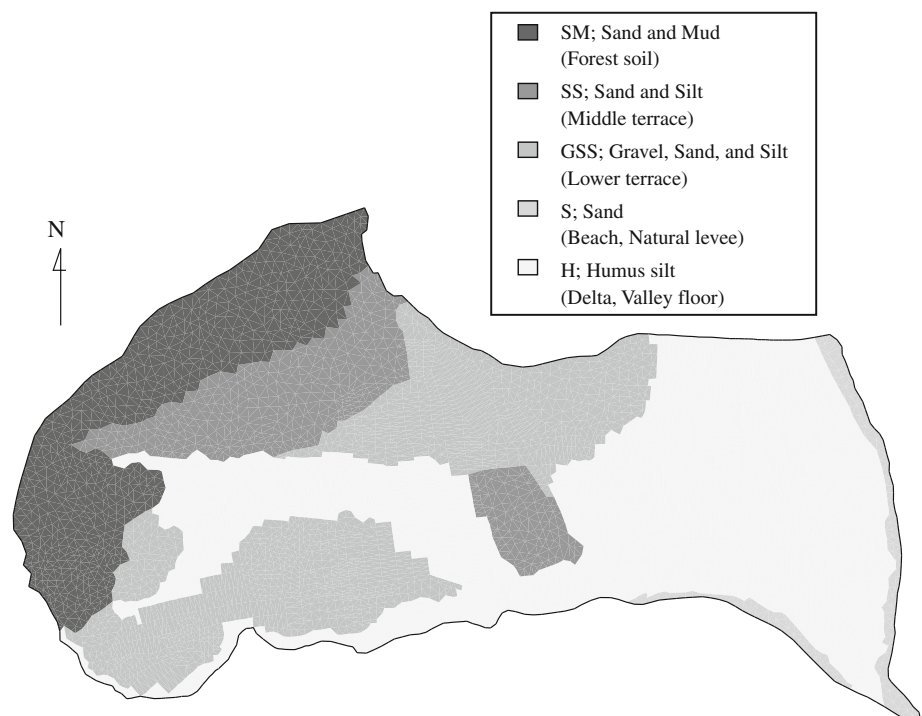
firstly estimated with linear interpolation and then revised with the temperature lapse rate of 0.065°C/m. The following rule for water management in paddy fields was considered. During an irrigation period of April 24 to July 31, all the paddy fields are ponded with an appropriate water depth except for a mid-summer drainage period. If the depth is reduced to 30 mm, irrigation water is supplemented considering the water requirements of 30 mm/day and 20 mm/day for rice paddies on the fan and the plain, respectively.

The ground surface elevation of each cell was identified from the digital map of 50×50 m grid. The surface geology was zoned with five soil types on the basis of the geological map (Nakae and Yoshioka 1998; Nakae et al. 2001), as shown in Fig. 6. The elevation of low-permeable layer, z_b, was assumed to vary according to the elevation of the ground surface so that the aquifer is 1.5 m thick in the forested hill and gradually becomes 5.5 m thick at the shore of the lake. For exception, the aquifer was assumed to be 10 m or more thick in the fan and the river terraces. The elevation of channel bed, z_r, was assumed to be 1.0–2.5 m lower than the ground surface on the basis of the survey results. The underdrain was assumed to be set only in the H zone (shown in Fig. 6), and its elevation, z_u, was assumed to be 1.0–2.0 m lower than the ground surface. The land use distribution is shown in Fig. 7, classified into forest, rice field and other crop field which includes the field converted from a rice field, housing land, irrigation tank and others.

The surface zone in the whole study area was meshed with 9,775 cells of triangular shape. The drainage canals shown in Fig. 7 were discretized into a total of 1,603 segments. For the open channel flow submodel, the external boundary conditions were given as follows. The volumetric flow rate given at the upstream end of drainage canal is that obtained from the in situ measurement. If the drainage canal feeds Lake Biwa, its end is regarded as the backwater-type downstream boundary, and otherwise, as the drop-type downstream boundary. A total of 6 diversion weirs, built across the main drainage canal for irrigation water intake, were treated as internal boundaries. The aquifer zone is discretized into 9,775 triangular cells and 1,603 rectangular cells. In the shallow groundwater flow submodel, the external boundaries formed by the ridge were treated as zero-flux Neumann boundaries, and those formed by the rivers and the lake shore were treated as Dirichlet boundaries with their water levels. The water levels of the rivers were assumed to correspond to their bed elevations with disregard for temporal variations of the water levels. The water levels of the lake were obtained from the web site of the Biwa Lake authority.

The initial conditions for all the submodels were provided by a warming-up calculation which is executed over the period of April 2008 to March 2009. The initial condition for the groundwater flow submodel, which is shown in Fig. 8, qualitatively consists with the actual distribution of the ground water level. In Fig. 8a, the inclination of the groundwater level is about 0.04 in the fan and is smaller than 0.01 in the plain. This is consistent with the observation aforementioned and shown in Fig. 5. In Fig. 8b, the depth to the groundwater table below the ground surface, the 'groundwater depth' mentioned here, is likely to be

Fig. 7 Land use distribution in 2009
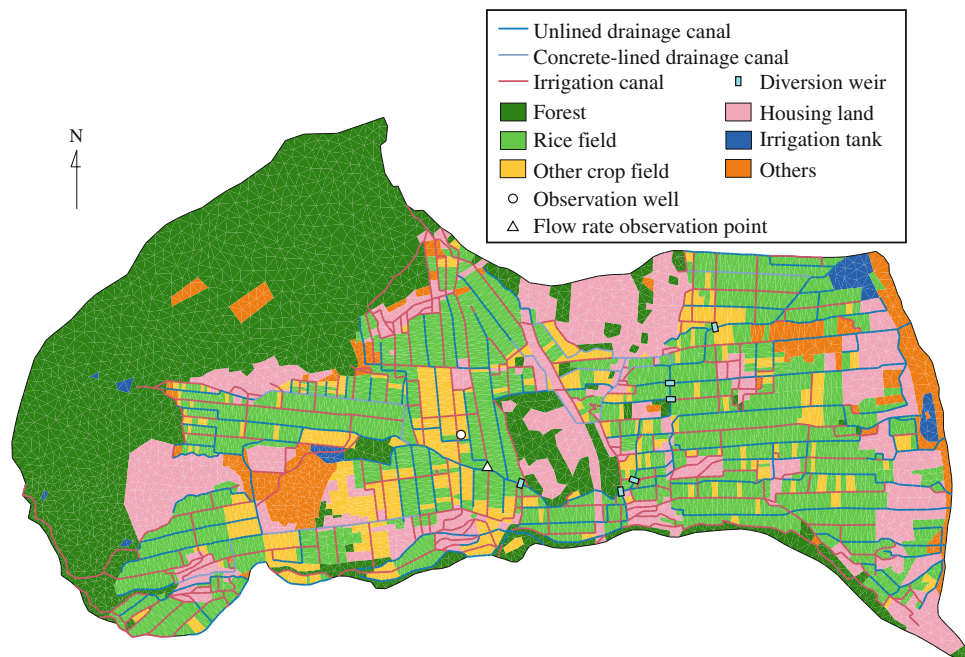
Fig. 8 Initial condition for
groundwater level.
(a groundwater level elevation
[m AMSL], b depth to
groundwater table below ground
surface [m])

(a)

(b)
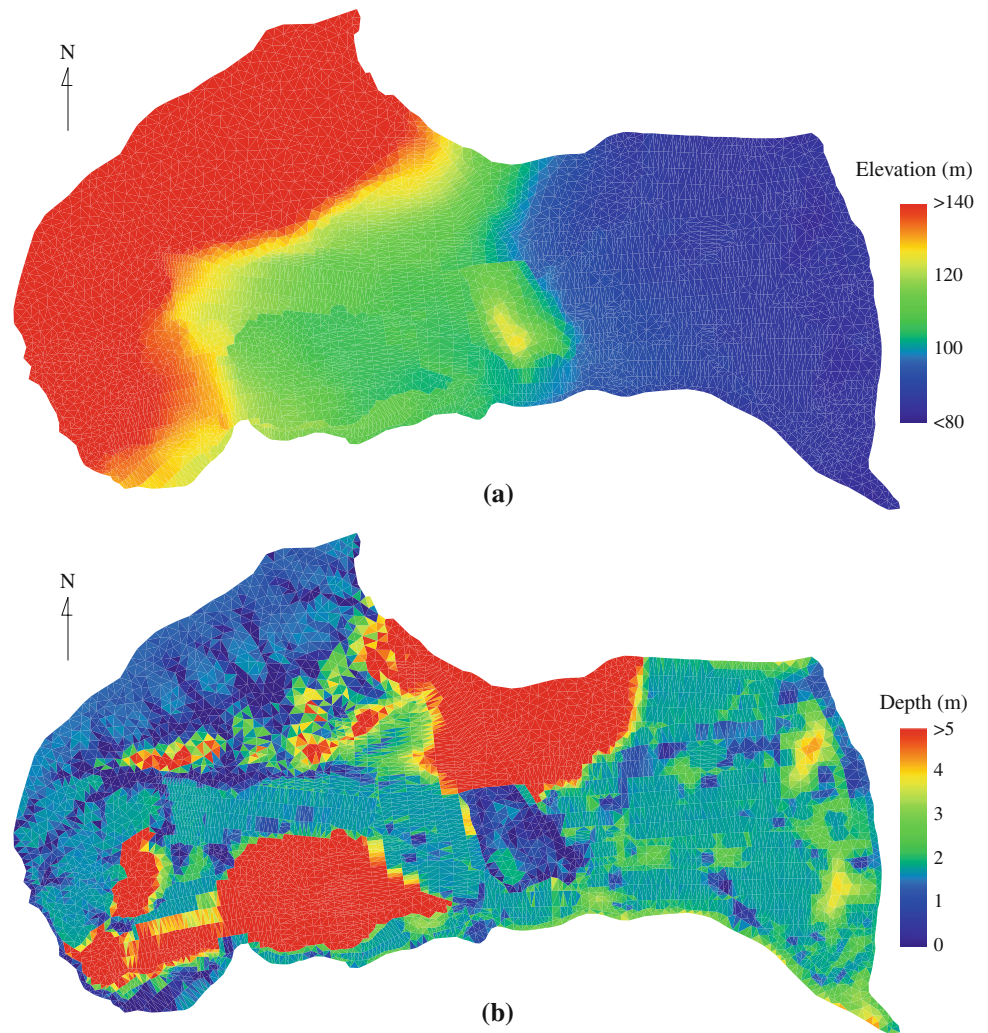
more than 3 m in the fan, while less than 2 m in the plain.
The groundwater level reaches the ground surface along
the mountain streams and the fringe of the forested hills.
This is consistent with the fact that spring spots are found
here and there in these areas.

Calibration and verification

The values of the model parameters common to both of the
previously developed HEWM-1 and the presently
improved HEWM-2 were identified to those given in the
earlier study (Takeuchi et al. 2010). The values of the
conceptual model parameters in the tank and soil moisture
submodels were determined, considering their physical
meanings and referring to the published studies (Alam
et al. 2006; Nakagiri et al. 1998). Their values were finally
identified through calibration of the model, so that the
reported amounts of evapotranspiration and groundwater
recharge (Lake Biwa Research Institute 1988; Mitsuno
and Nagahori 1987) were reproduced by the model. The
values of the physical model parameters in the shallow

groundwater submodel, the two left columns in Table 1,
were inferred from field tests, laboratory tests and the lit-
eratures. The hydraulic conductivities for the two soil types

Table 1 Parameters of groundwater flow submodel

Geological zone	K $(10^{-3}$ cm/s)	n^e (–)	K_{zr} $(10^{-3}$ cm/s)	L_{zr} (m)	κ (m^{-1})
SM	1.00	0.70	–	–	–
SS	1.80	0.49	–	–	–
GSS	1.80	0.49	0.54	0.1	1.0
S	0.10	0.35	0.03	0.2	1.0
H	0.77	0.40	0.23	0.2	1.0

Table 2 Parameters of open channel flow submodel

| Type of drainage canal	n_M (–)
Concrete-lined	0.016
Unlined	0.020

in the alluvial fan and the alluvial plain (GSS and H zones shown in Fig. 6) were in situ measured as aforementioned, and their porosities were estimated from the core samples as well. The values of the hydraulic conductivity and the porosity for other soil types were estimated referring to Linsley et al. (1958) and Domenico and Mifflin (1965).

The values of the model parameters newly introduced in this study were identified in the following manner. The values of the melting coefficient, m, estimated by Kojima et al. (1983) were employed as they are 0.14 mm/(°C h) from November to January and 0.21 mm/(°C h) from February to March. In the open channel flow submodel, the Manning's roughness coefficient, n_M, was estimated from the literature and model calibration, as shown in Table 2: 0.016 for concrete-lined canals and 0.020 for unlined canals. In the groundwater submodel, the thickness and the hydraulic conductivity of the canal bed stratum, L_{zr} and K_{zr}, were inferred through model calibration, as shown in Table 1. Since the elevation of stratum bottom is a critical level at which surface water and groundwater becomes disconnected, the stratum thickness is thought to be larger than an air entry pressure head of the aquifer soil. The value of L_{zr} on the H zone (shown in Fig. 6) was identified to be 0.2 m, while that on the GSS zone to be 0.1 m. The value of K_{zr} was identified to be 30% of K: 2.3×10^{-4} cm/s for the canals on the H zone and 5.4×10^{-4} cm/s on the GSS zone. The discharge coefficient for the underdrains, κ, was identified as 1.0 with model calibration, as shown in Table 1.

The parameter identifications, executed above, resulted from calibrating the model by comparison of the computed and observed flow rates in the drainage canal and that of the computed and observed groundwater levels. In calibration, the reproducibility of the computed result was measured in terms of statistics, and a particular simulation run which minimizes the residuals was found on a trial and error basis. For the calibration, the simulations were run with the data from April 2010 to November 2010, because the data of the canal flow rate before April 2010 were not available at all. Using the identified parameter values, verification of those values was done with the data of another time period from April 2009 to March 2010.


Fig. 9 Computed and observed volumetric flow rates in canal
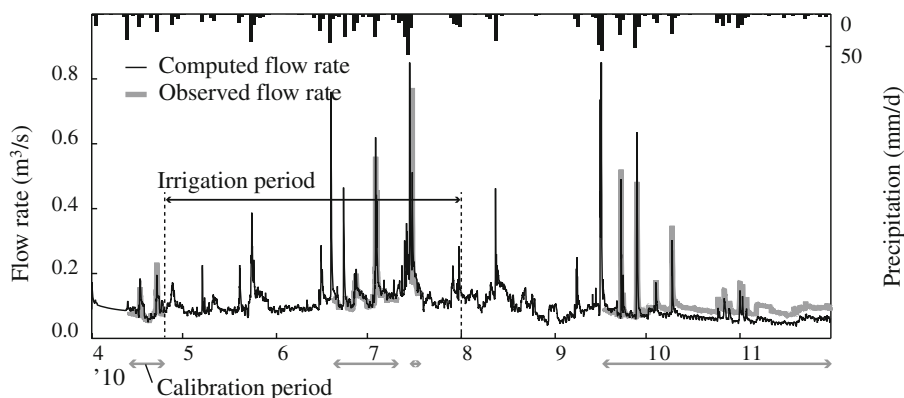
Table 3 Statistics for the calibration/verification performance

Measures	Q (calibration)	H_g (calibration)	H_g (verification)
Scaled mean sum of residuals [%]: $\mathrm{SMSR} = \frac{100}{n\Delta Y} \sum_{i=1}^{n} |y_i - Y_i|$	1.7	14	13
Scaled root mean fraction square [%]: $\mathrm{SRMFS} = \frac{100\overline{Y}}{\Delta Y} \sqrt{\frac{1}{n} \sum_{i=1}^{n} \left(\frac{y_i - Y_i}{Y_i}\right)^2}$	2.0	17	16
Scaled root mean square [%]: $\mathrm{SRMS} = \frac{100}{\Delta Y} \sqrt{\frac{1}{n} \sum_{i=1}^{n} (y_i - Y_i)^2}$	2.1	17	16
Root mean square [m³] or [m]: $\mathrm{RMS} = \sqrt{\frac{1}{n} \sum_{i=1}^{n} (y_i - Y_i)^2}$	0.03	0.06	0.05
Correlation coefficient [–]: $r = \frac{\sum_{i=1}^{n} (y_i - \overline{y})(Y_i - \overline{Y})}{\sqrt{\sum_{i=1}^{n} (y_i - \overline{y})^2} \sqrt{\sum_{i=1}^{n} (Y_i - \overline{Y})^2}}$	0.80	0.44	0.56

n number of values, y computed value, Y observed value, ΔY range of Y, $\overline{y}$ mean of y, $\overline{Y}$ mean of Y
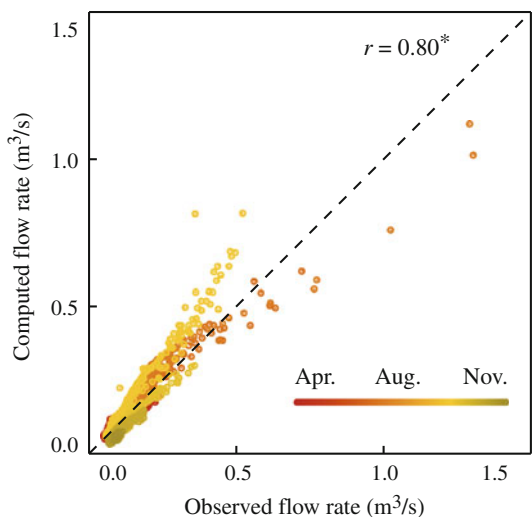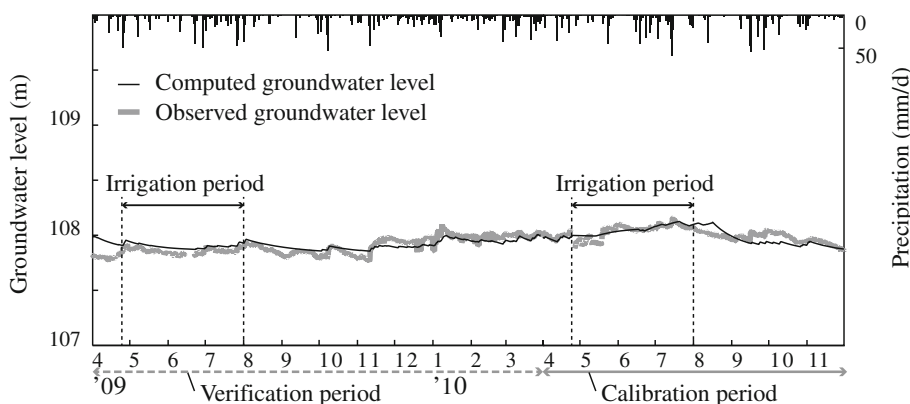
Fig. 10 Scattergram of observed versus computed flow rates

Figure 9 comparatively illustrates the time-varying computed and observed canal flow rates at the observation point (depicted in Fig. 7). It shows some interruptions in

the observed flow rates, because the observed data are often lacked. The values of the calibration performance measures that are integrated over the four broken sub-periods (denoted in Fig. 9) are listed in Table 3. The values of RMS (Root Mean Square), SRMS (Scaled RMS), SRMFS (Scaled Root Mean Fraction Square) and SMSR (Scaled Mean Sum of Residuals) are sufficiently low, and the value of correlation coefficient, r, is adequately high. The temporal distribution of the residuals (the difference between observed and computed levels) is also checked with a scattergram of observed and computed flow rates, as shown in Fig. 10. It suggests that peak flow rates tend to be under-predicted with this model, especially when the flow rate is over 1.0 m³/s.

Figure 11 comparatively illustrates the time-varying computed and observed groundwater levels at the observation well. It shows that the computed groundwater level roughly trace the observed one. The values of SRMS, SRMFS and SMSR are over 10%, and the value of r is not high, as shown in Table 3. The scattergram (Fig. 12) indicates that the residuals are adequately low over the whole period except for April, 2009. The over-predicted
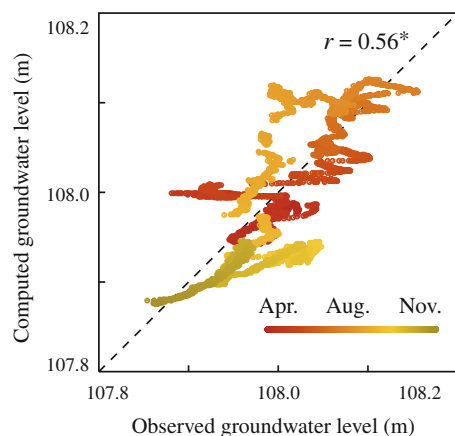
Fig. 11 Computed and observed groundwater levels

Fig. 12 Scattergram of observed versus computed groundwater levels. **a** Calibration period, **b** Verification period
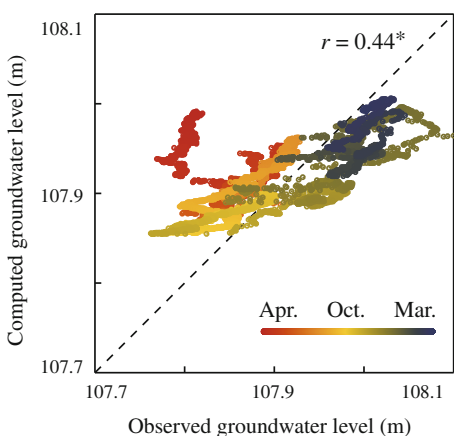
groundwater levels in April, 2009, which resulted from an over-predicted initial condition, might cause the poor values of the performance measures above mentioned. Although there is still room for improvement, the results of model calibration are generally acceptable. For better model calibration performance, some additional data are needed to give information about the spatial distributions of groundwater level and canal flow rate.

Results and discussion

Table 4 shows the annual water budget over the whole area, which was calculated from the result of the numerical flow simulation during the 1-year period of April 2009 to March 2010. The net income to the surface zone, obtained from deduction of the evapotranspiration loss from the total water supply by rainfall/snowfall and irrigation (or the sum of the values with a superscript (a) in Table 4), is 1,367 mm/y. Since the recharge from the surface zone to the aquifer zone (superscript (b)) is 920 mm/y, it accounts for 67% of the net income on the surface zone. The corresponding percentage of the recharge was 61% in the earlier study (Takeuchi et al. 2010) which applied HEWM-1 for the other period of April 2006 to March 2007. On the aquifer zone, the surface-to-aquifer recharge (920 mm/y, superscript (c)) account for 92% of the total groundwater

recharge to the aquifer (1,002 mm/y, superscript (d)). The similar percentage, 96%, was obtained in the earlier study (Takeuchi et al. 2010). The water returning from the aquifer to the surface zone, which consists of the spring and the discharge to the canals and the rivers (or the sum of the values with a superscript (e), 499 mm/y), accounts for 54% of the recharge (920 mm/y, superscript (c)). According to Sato et al. (2007), who developed the water quality model consisting of surface water and groundwater submodels, the simulation result for the whole Lake Biwa watershed showed that annual groundwater recharge accounts for 60% of the net income (deduction of evapotranspiration from sum of rainfall and irrigation). Their study also shows that the water returning from the aquifer to the surface is 39% of the groundwater recharge. Our result in water budget is nearly consistent with their result despite many differences between the two models.

Figure 13 compares the cumulative surface water and groundwater discharges to canals over-a-year. Note that the groundwater discharge corresponds to the canal-aquifer flow rate, which is the sum of the exchange flow rate through canal bed and the underdrain discharge. The surface discharge is highly susceptible to erratic rainfall/snowfall, while the groundwater discharge is rather subject to gradual rise and fall of the groundwater table 43% of the gross discharge throughout-a-year (1.1×10^7 m³/y) is of groundwater origin.

Table 4 Annual water budget in whole area

Surface zone	Rain & Snow	Irrigation	Evapotranspiration	Canals	Rivers & Lake	Recharge	Spring	Total
Income	1483	499	–	–	–	–	105	2087
Outgo	–	–	615	502	50	920[b]	–	2087
In–Out	1483[a]	499[a]	−615[a]	−502	−50	−920	105	0

Aquifer zone	Recharge	Spring	Canals	Sakai Riv.	Ishida Riv.	Biwa Lake	Leakage	Total
Income	920[c]	–	39	43	0	0	–	1002[d]
Outgo	–	105	381	69	26	4	372	957
In–Out	920	−105[e]	−342[e]	−26[e]	−26[e]	−4	−372	45

Superscript a–e: defined in text

**Fig. 13** Cumulative surface water/groundwater discharge
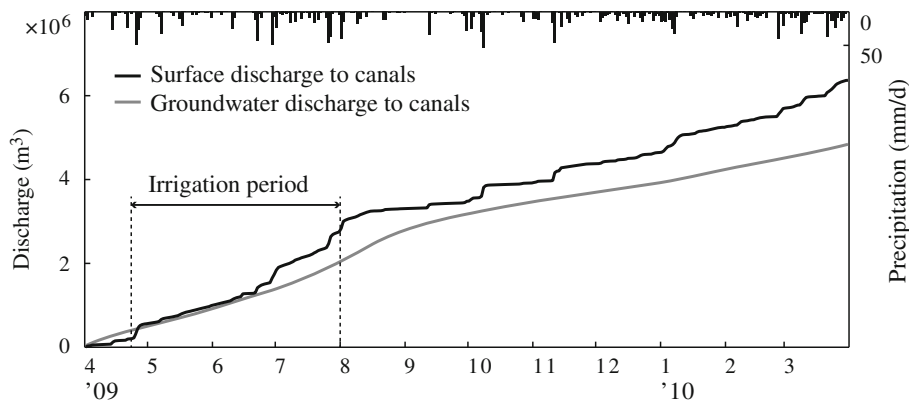
Fig. 14 Time-varying canal-aquifer flow
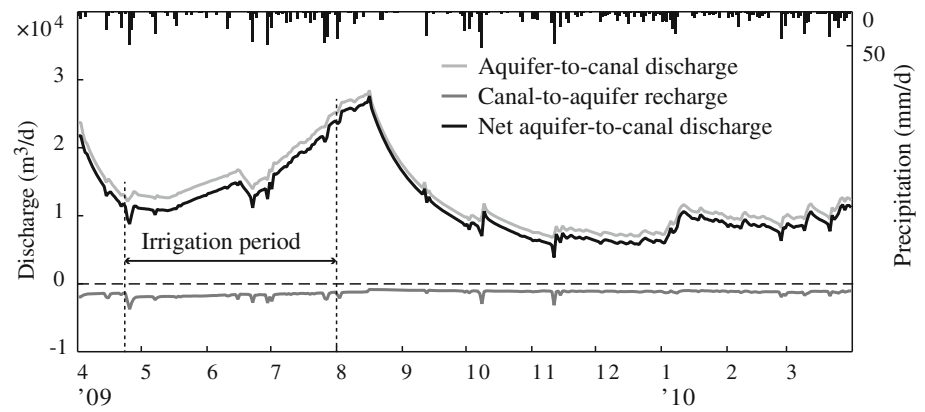
The interactive canal-aquifer flow dynamics, integrated over all the drainage canals, is illustrated in Fig. 14. It includes annual variations of the aquifer-to-canal discharge, the canal-to-aquifer recharge (reverse or negative discharges) and the net aquifer-to-canal discharge. The discharge peaks late after the termination of the irrigation period and reaches the bottom in autumn. This annual variation of the discharge corresponds to that of the groundwater level. The temporal increasing events of the recharge are thought to be caused by sharp rises of in-canal

Fig. 15 Distributions of groundwater depth and canal-aquifer flow rate. **a** November, 2009, **b** July, 2010
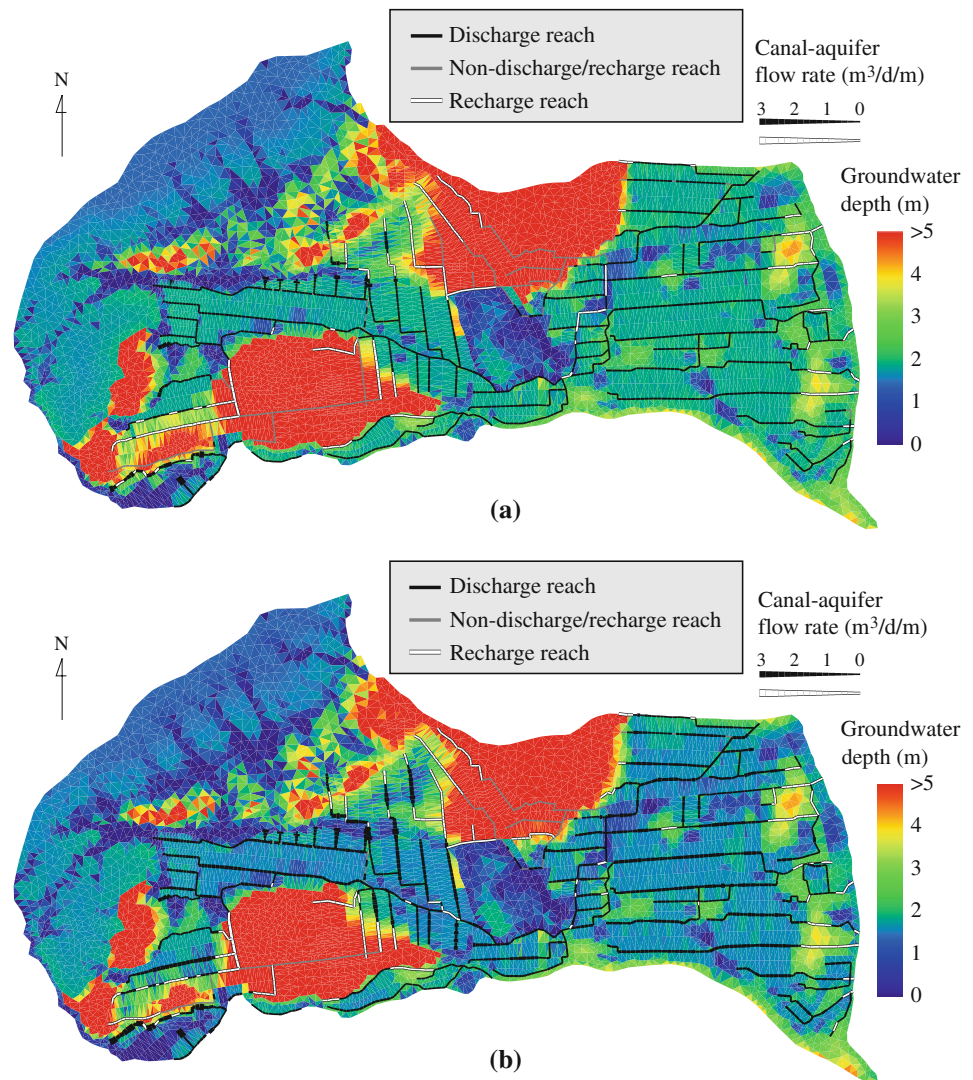
water level, because they were not found in the simulation with HEWM-1 (Takeuchi et al. 2010). The effect of canal rise on recharge can be simulated with HEWM-2 because of the open channel flow submodel newly introduces.

Figure 15 visualizes the spatial distributions of the groundwater depth and the canal-aquifer flow rate, in winter (November) and summer (July) seasons. The discharge reach indicates a reach of the canal which gains groundwater discharged from aquifer. The recharge reach is a reach which loses stream water to recharge groundwater. In both the seasons, the groundwater depth is likely to be more than 3 m in the fan, while less than 2 m in the plain. The drainage canals in the fan and the plain mostly serve as losing and gaining canals, respectively. At the upstream side of the diversion weirs, the canal loses water despite high groundwater level, because the weirs keep the in-canal water level higher than the groundwater level. In summer when groundwater depth becomes less than 1.5 m in a wide area of the plain, most of the drainage canals gain the discharge of 2–3 m^3/d/m. For better model application, the physical properties (e.g. depth, inclination and permeability of bottom sediment) of all canals need to be investigated.

Conclusion

This study improves HEWM-1 so that the improved model, HEWM-2, can simulate the dynamic canal-aquifer interaction caused by the rise and fall of the difference between surface water level and groundwater level. In HEWM-2, the time-varying surface water level is computed to determine the direction (discharging or recharging) and the rate of the canal-aquifer flow for any canal at each time step. HEWM-2 has the following improvements on HEWM-1:

- Open channel flow submodel is introduced in which the stream flow in the canals is represented by the complete 1-D shallow water equations.
- Different two effects of canal-aquifer flow are explicitly represented. The exchange flow through canal bed is represented with Eqs. 13 and 14, and the underdrain discharge is done with Eq. 15.
- In meteorological description, an empirical snow melting model is introduced so that snowfall is distinguished from rainfall to melt and infiltrate soil with some lags.

With an integrated operation of the four submodels, the hydro-environmental aspects of a watershed can be investigated numerically at a field-plot-scale resolution.

The validity of HEWM-2 was qualitatively shown, though it is difficult to verify the simulation results with the spatial distributions of groundwater level and canal-aquifer

interaction because of the limitation of available observation data. This model is efficacious for assessing irrigation impacts on hydrological cycle in detail and for implementing integrated management of agricultural canal systems. The model could also be a useful tool for identifying whether any drainage canal is gaining or losing water in relation to groundwater level, and at the same time for estimating the canal-aquifer flow rate. If maps of such canal attributes associated with canal-aquifer interaction are provided, as shown for the application example, these could assist in conserving a complex network of drainage canals which is biological corridor for aquatic animals like fishes.

References

Alam AHMB, Takeuchi J, Kawachi T (2006) Development of distributed rainfall-runoff model incorporating soil moisture model. Trans JSIDRE 244:29–37

Asai K, Hosoda T (1999) Numerical analysis for convection equation. Lecture note for computer applications in hydraulic engineering, pp 13–21 (in Japanese)

Brath A, Montanari A, Toth E (2004) Analysis of the effects of different scenarios of historical data availability on the calibration of a spatially-distributed hydrological model. J Hydrol 291:232–253

Carroll RWH, Pohll G, McGraw D, Garner C, Knust A, Boyle D, Minor T, Bassett S, Pohlmann K (2010) Mason valley groundwater model linking surface water and groundwater in the walker river Basin, Nevada. J Am Water Resour Assoc 46(3):554–573

Domenico PA, Mifflin MD (1965) Water from low permeability sediments and land subsidence. Water Resour Res 1(4):563–576

Fujihara M, Ohashi G (2000) A numerical estimation of the effect on groundwater surface elevation by irrigation water in Dogo Plain. Trans JSIDRE 208:155–163 (in Japanese)

Fujinawa K (1981) The role of water for agricultural use as the source of groundwater recharge; analysis of groundwater in Nasuno-gahara Basin by a mathematical model. Bull Natl Res Inst Agric Eng Jpn 21:127–141 (in Japanese)

Hu L-T, Chen C-X, Jiao JJ, Wang Z-J (2007) Simulated groundwater interaction with rivers and springs in the Heihe river basin. Hydrol Process 21:2794–2806

Imaizumi M, Ishida S, Tuchihara T (2006) Long-term evaluation of the groundwater recharge function of paddy fields accompanying urbanization in the Nobi Plain, Japan. Paddy Water Environ 4:251–263

Japan Meteorological Agency (2011) Statistics of automated meteorological data acquisition system for Imazu station (online). Available from: http://www.data.jma.go.jp/obd/stats/etrn/index.php. Accessed 3 Jan 2011 (in Japanese)

Jia Y, Ni G, Kawahara Y, Suetsugi T (2001) Development of WEP model and its application to an urban watershed. Hydrol Process 15:2175–2194

Kim NW, Chung IM, Won YS, Arnold JG (2008) Development and application of the integrated SWAT-MODFLOW model. J Hydrol 356:1–16

Kojima K, Motoyama H, Yamada Y (1983) Estimation of melting rate of snow by simple expression using only air temperature. Low Temp Sci A Phys Sci 42:101–110 (in Japanese)

Korkmaz S, Ledoux E, Önder H (2009) Application of the coupled model to the Somme river basin. J Hydrol 366:21–34

Krause S, Bronstert A (2007) The impact of groundwater-surface water interactions on the water balance of a mesoscale lowland river catchment in northeastern Germany. Hydrol Process 21:169–184

Lake Biwa Research Institute (1988) Moving Atlas-Shiga prefecture regional environment atlas with data floppy disc (in Japanese)

Linsley RK, Kohler MA, Pauthus JLH (1958) Hydrology for engineers. McGraw-Hill, New York, NY

Liu CW, Tan CH, Huang CC (2005) Determination of the magnitudes and values for groundwater recharge from Taiwan's paddy field. Paddy Water Environ 3:121–126

Matsuo T (1984) The study of melting of snowflakes in the atmosphere. Tech Rep Meteorol Res Inst 8:10–20 (in Japanese)

McDonald MG, Harbaugh AW (1988) A modular three-dimensional finite-difference ground-water flow model. U.S. Geological Survey Techniques of Water-Resources Investigations, Book 6, chap. A1

Mitsuno T, Nagahori K (1987) The structure of groundwater budget around Yoshii Weir-Statistical analysis of observed groundwater level fluctuations around Yoshii Weir. Trans JSIDRE 127:27–33 (in Japanese)

Nakae S, Yoshioka T (1998) Geology of the Kumagawa District. Geological Survey of Japan (in Japanese)

Nakae S, Yoshioka T, Naito K (2001) Geology of the Chikubu-Shima District. Geological Survey of Japan (in Japanese)

Nakagiri T, Watanabe T, Horino H, Maruyama T (1998) Development of a hydrological system model in the Kino River Basin—analysis of irrigation water use by a hydrological system model (I). Trans JSIDRE 198:1–11

Prickett TA, Lonnquist CG (1971) Selected digital computer techniques for groundwater resource evaluation. Bulletin 55, Urbana

Prudic DE (1989) Documentation of a computer program to simulate stream-aquifer relations using a modular, finite-difference ground-water flow model. U.S. Geological Survey Open-File Report, 88-729

Prudic DE (2004) A new Streamflow-Routing (SFR1) package to simulate stream-aquifer interaction with MODFLOW-2000. U.S. Geological Survey Open-File Report, 2004-1042

Rushton KR, Tomlinson LM (1979) Possible mechanisms for leakage between aquifers and rivers. J Hydrol 40(1–2):49–65

Sato Y, Kim J, Takada T, Naito M, Nagare H, Komatsu E, Uehara H (2007) Development of water quality model for Lake Biwa Basin and its application for environmental assessment. Annu Rep Lake Biwa Environ Res Inst 3:43–46

Schaffranek RW, Baltzer RA, Goldberg DE (1981) A model for simulation of flow in singular and interconnected channels. U.S. Geological Survey Techniques of Water-Resources Investigations, Book 7, chap. C3

Sophocleous M (2002) Interactions between groundwater and surface water the state of the science. Hydrogeol J 10(1):52–67

Sugawara M, Ozaki E, Watanabe I (1986) River forecasting of the upper Irrawaddy River at Sagaing, Burma, using the tank model. Rep Natl Res Center Disaster Prev 36:47–57

Swain ED, Wexler EJ (1996) A coupled surface-water and ground-water flow model (MODBRNCH) for simulation of stream-aquifer interaction. U.S. Geological Survey Techniques of Water-Resources Investigations, Book 6, chap. A6

Takeuchi J, Kawachi T, Unami K, Maeda S, Izumi T (2009) A distributed hydro-environmental watershed model with three-zoned cell profiling. Paddy Water Environ 7:33–43

Takeuchi J, Imagawa C, Kawachi T, Unami K, Maeda S, Izumi T (2010) A refined hydro-environmental watershed model with field-plot-scale resolution. Paddy Water Environ 8:175–187

Tan BQ, O'Connor KM (1996) Application of an empirical infiltration equation in the SMAR conceptual model. J Hydrol 185:275–295

Thompson JR, Sørenson HR, Gavina H, Refsgaard A (2004) Application of the coupled MIKE SHE/MIKE 11 modelling system to a lowland wet grassland in southeast England. J Hydrol 293(1–4):151–179

Wakasa M (2006) Groundwater environment and recharge function of irrigation soil canals: a study in Minase alluvial fan, Akita Prefecture. Geogr Rev Akita Univ 53:33–36 (in Japanese)